
Generalized Logit Adjustment: Calibrating Fine-tuned Models by Removing Label Bias in Foundation Models

Beier Zhu¹ Kaihua Tang¹ Qianru Sun² Hanwang Zhang¹
¹Nanyang Technological University ²Singapore Management University
beier002@e.ntu.edu.sg, hanwangzhang@ntu.edu.sg

Abstract

Foundation models like CLIP allow zero-shot transfer on various tasks without additional training data. Yet, the zero-shot performance is less competitive than a fully supervised one. Thus, to enhance the performance, fine-tuning and ensembling are also commonly adopted to better fit the downstream tasks. However, we argue that such prior work has overlooked the inherent biases in foundation models. Due to the highly imbalanced Web-scale training set, these foundation models are inevitably skewed toward frequent semantics, and thus the subsequent fine-tuning or ensembling is still biased. In this study, we systematically examine the biases in foundation models and demonstrate the efficacy of our proposed Generalized Logit Adjustment (GLA) method. Note that bias estimation in foundation models is challenging, as most pre-train data cannot be explicitly accessed like in traditional long-tailed classification tasks. To this end, GLA has an optimization-based bias estimation approach for debiasing foundation models. As our work resolves a fundamental flaw in the pre-training, the proposed GLA demonstrates significant improvements across a diverse range of tasks: it achieves 1.5 pp accuracy gains on ImageNet, a large average improvement (1.4-4.6 pp) on 11 few-shot datasets, 2.4 pp gains on long-tailed classification. Codes are in <https://github.com/BeierZhu/GLA>.

1 Introduction

Thanks to the Web-scale data and self-supervised strategies, foundation models like CLIP [40] empower zero-shot transfer to a wide variety of domains [7, 1, 52]. However, the zero-shot performance is still weak on several domain-specific tasks such as differentiating models of cars, species of flowers, and variants of aircraft [40, 7]. Therefore, it is a common practice to improve the downstream performance via supervised fine-tuning on labeled data, *e.g.*, linear probing, prompt tuning [54, 55], and end-to-end fine-tuning.

However, fine-tuned models are easily biased: they are adept in exploiting spurious correlations that only hold on the downstream distribution [40, 39, 48, 55]. To improve the robustness, several studies [48, 55, 56] propose to combine fine-tuned models with zero-shot models. For example, WiSE-FT [48] ensembles the fine-tuned and zero-shot models in weight space and ProGrad [55] uses zero-shot predictions to regularize the fine-tuning gradient. The underlying assumption lies in that the zero-shot models are robust to distribution shifts [40], and their predictions are complementary to those of fine-tuned models [48].

Despite these methods exhibiting performance gains on both in-distribution and out-of-distribution evaluations, they all overlook the inherent bias originating from the foundation models. Specifically, the Web-scale data for pre-training foundation models exhibit a highly skewed distribution due to Zipf’s law of nature [42]. The resulting foundation models develop a biased decision boundary that leads to a poor zero-shot performance on rare classes. As evidenced in Figure 1(a) and (b), the purple

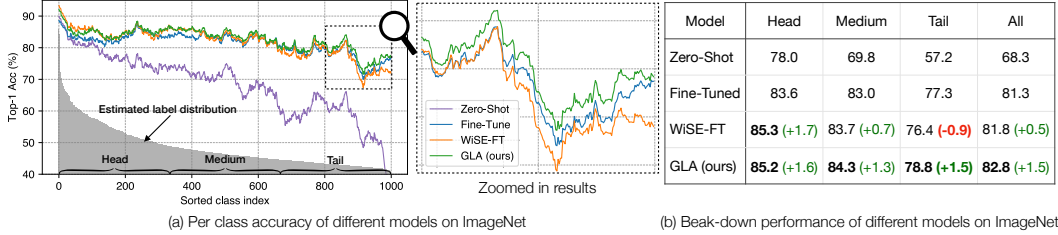


Figure 1: (a) Per class accuracy of CLIP-ViT/B16 on ImageNet. Class index are sorted using the estimated pre-training label prior. Curves are smoothed for better visualization. (b) Beak-down performance of different models on ImageNet. We equally divide the ImageNet classes into three subgroups, according to the class index. Existing ensemble methods like WiSE-FT [48] exhibits a clear performance loss on tail classes, while our GLA stands out for all three subgroups.

line encounters a dramatic drop, and the zero-shot performance of tail classes is significantly lower than that of head classes (57.2% vs. 78.0%). Existing ensemble methods like WiSE-FT [48] overlook the label bias, resulting in an improvement in top-1 (+0.5%) and head accuracy (+1.7%) while a noticeable degradation on the tail performances (-0.9%) in Figure 1(b). Another evidence is that the orange line (WiSE-FT) is below the blue line (fine-tuned models) for rare classes in Figure 1(a).

We propose Generalized Logit Adjustment (GLA), a simple post-hoc method consisting of two steps: **1)** removing the label bias of zero-shot model via estimating the label distribution in the pre-training dataset; **2)** ensembling the fine-tuned and debiased zero-shot models. As illustrated in Figure 1 (b), our GLA achieves consistent improvement across all three subgroups, particularly showing a significant gain on tail classes (+1.5%). Despite its simplicity, our GLA has a firm statistical grounding: it is the Bayes optimal classifier given the fine-tuned and zero-shot models, thus consistent for minimizing the error on a class-balanced target distribution (Section 4.2). It is worth noting that removing the bias of foundation models is challenging since the label distribution is often inaccessible due to privacy or copyright concerns. In this work, we only use the downstream labeled data and the zero-shot model to estimate the foundation label bias. Specifically, we formulate the problem by adjusting the margin of the zero-shot models such that the lowest error is achieved on the downstream dataset. This grounding translates into strong empirical performance on real-world datasets, covering few-shot, many-shot, and long-tail learning (Section 5).

The contributions and novelties of this work are summarized as follows:

- We point out the overlooked label bias in foundation models, which originates from the skewness of pre-training distribution that affects the performance of downstream tasks.
- We formalize the estimation of the label bias as a constrained optimization problem (Section 3.2) with theoretical justification (Section 4.3). The entire process does not require access to the pre-training dataset, making it practical for fine-tuning scenarios. We present Generalized Logit Adjustment (GLA) method, which ensembles the debiased zero-shot and fine-tuned models, and demonstrate its superiority over conventional fine-tuning and ensembling by proving it’s a Bayes optimal classifier (Section 4.2).
- We build a comprehensive benchmark for evaluation, which considers three real-world settings and three fine-tuning paradigms. The settings are: 1) many-shot learning with abundant data 2) few-shot learning; and 3) long-tail classification, representing a more challenging scenario that combines many-shot and few-shot data (Section 5). The three fine-tuning paradigms include: 1) end-to-end fine-tuning; 2) linear probing; and 3) prompt tuning (Section 3.1).
- We demonstrate the efficacy of our proposed method GLA by conducting extensive experiments across various settings and fine-tuning paradigms. We observe 1 to 1.5 pp accuracy gains on ImageNet, large averaged improvement (1.4 to 4.6 pp) on 11 few-shot datasets and 2.4 pp averaged accuracy gains on long-tail datasets. (Section 5).

2 Related Work

Image-text foundation models. Foundation models pre-trained by contrastive objectives have set impressive milestones for image and text representation learning, with CLIP [40], ALIGN [23], CoCa [52] and Flamingo [1] being the exemplars. Such models exhibit impressive prompt-based zero-shot performance on various image recognition downstream tasks. Our method aims to reduce foundation model biases to boost performance in downstream tasks. While [2] also addresses word frequency bias, we differ in two key areas: Firstly, we debias zero-shot models using fixed prompts, whereas [2] refines the prompting process. Secondly, our GLA doesn't require access to a subset of the pre-training data.

Ensembles. Ensemble methods aim to boost performances by combining multiple networks, which can be either implemented by aggregating model outputs [12, 4, 28, 14, 27, 51], weight-space ensembling [48, 22], or ensemble distillation [19, 29]. For the adaptation of foundation models, several work propose to ensemble the fine-tuned and zero-shot models for better performance: Wortsman et al. [48] ensembles them in weight space; ProGrad and ProReg [55, 56] propose to fuse them via knowledge distillation. Our GLA is orthogonal to these approaches, as it concentrates on mitigating the biases in foundation models that are detrimental to ensemble models.

Logit adjustment. Logit adjustment [35, 45, 24, 49, 20] is a post-hoc technique to adjust the biased output of classification networks. Kang et al [24] proposes an element-wise scaling adjustment for the classifier weight. Tang et al [45] removes the projection of features on a global biased direction. Menon [35] derives the theoretically optimal adjustment from the training distribution. Unlike the those approaches which rely on a transparent training data or class distribution, our GLA can eliminate the class bias without accessing to the pre-training statistics.

3 Methods

3.1 Setup

Task. Consider a classification problem with instances $\mathbf{x} \in \mathcal{X}$ and labels $y \in \mathcal{Y} = [K] = \{1, \dots, K\}$. We have a zero-shot model f_{zs} (given below), a downstream dataset $\mathcal{D}_s = \{\mathbf{x}_i, y_i\}_{i=1}^{N_s}$ drawn from source distribution P_s and a fine-tuned model f_{ft} (given below) trained on the dataset \mathcal{D}_s . Give a model $f : \mathcal{X} \rightarrow \mathbb{R}^K$ that outputs prediction score, we define the risk of f on the target distribution P_t as the mis-classification rate: $\mathcal{R}_t(f) = \mathbb{E}_{\mathbf{x}, y \sim P_t} [y \neq \arg\max_i f(\mathbf{x})_i]$. Our goal is to learn a model f_{gla} that best leverages f_{zs} and f_{ft} that minimizes the risk \mathcal{R}_t .

Zero-shot models. We primarily explore CLIP [40] for zero-shot models. CLIP consists of a visual encoder $\Phi_v(\mathbf{x})$ and a text encoder $\Phi_t(\mathbf{t})$, producing l_2 -normalized features from an image \mathbf{x} and a text \mathbf{t} respectively. Zero-shot model f_{zs} for K classes is enabled by matching image features $\mathbf{v} = \Phi_v(\mathbf{x})$ with classification weights $\mathbf{w}_k = \Phi_t(\mathbf{t}_k)$, where \mathbf{t}_k is obtained by extending the class name $\{c_k\}$ to a pre-defined prompt, e.g., "a photo of a $\{c_k\}$.". Additional details are provided in Appendix B.2. The probability of \mathbf{x} being classified as y is defined as:

$$P(y|\mathbf{x}) = \text{softmax}(f_{zs}(\mathbf{x}))_y = \frac{\exp(\mathbf{v}^T \mathbf{w}_y)}{\sum_{k=1}^K \exp(\mathbf{v}^T \mathbf{w}_k)}. \quad (1)$$

Fine-tuned models. Standard fine-tuning initializes the model f_{ft} with the pre-trained parameters and then solve $f_{ft} = \arg\min_f \mathcal{R}_s(f)$ to minimize the risk on downstream dataset. We consider three common variants of fine-tuning: (1) end-to-end, where all parameters of Φ_v and \mathbf{w}_k are updated; (2) linear probing, where only \mathbf{w}_k is modified while Φ_v is fixed; (3) prompt tuning, where the text input \mathbf{t}_k is learned, while keeping Φ_v and Φ_t freezed. See Appendix B.3 for details on fine-tuning methods.

Notation. Let $P_p(y)$, $P_s(y)$ and $P_t(y)$ be the marginal probability of class $y \in [K]$ for pre-training, source (training) and target (test) distribution, respectively. Let π_p and π_s denote the log probabilities of class for pre-training and training distribution, i.e., $\pi_p(y) = \log P_p(y)$ and $\pi_s(y) = \log P_s(y)$.

3.2 Generalized Logit Adjustment Framework

Fine-tuned models often yield significant gains compared to zero-shot models, and ensembling them can further improve performance. This leads to a natural question: How should we best leverage

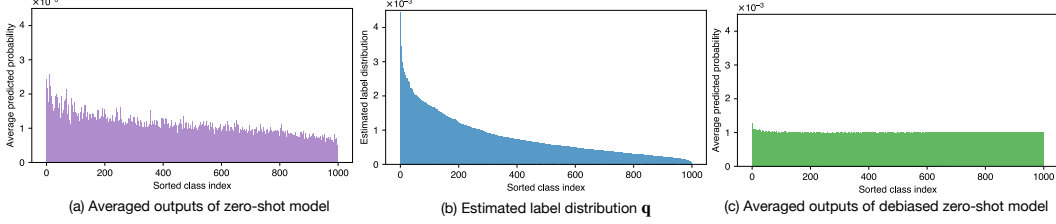


Figure 2: Illustration of debiasing process on ImageNet validation set. (a) The original distribution of zero-shot outputs; (b) the estimated pre-train distribution \mathbf{q} based on our algorithm; (c) the distribution of debiased zero-shot outputs using estimated \mathbf{q} .

the zero-shot and fine-tuned models for the prediction tasks? We attempt to answer by proposing generalized logit adjustment in Definition 1.

Definition 1. (GLA) The Generalized Logit Adjustment (GLA) model f_{gla} is defined as follows:

$$f_{\text{gla}}(\mathbf{x}) = f_{\text{ft}}(\mathbf{x}) + f_{\text{zs}}(\mathbf{x}) - \pi_s - \pi_p. \quad (2)$$

In Section 4.2, we prove that given the zero-shot and fine-tuned models, our GLA model is the *Bayes* optimal classifier and no other combination of the two models can outperform it. Here remains one important question: how could we obtain π_p as we have no access to the pre-training statistics? We provide the estimation process of π_p in Eq (4) and postpone the justification in Section 4.3. The entire GLA algorithm consists of two steps which is given as follows:

Step 1: Estimation of π_p . Let \mathbf{q} be an arbitrary *probability simplex* over K classes. Given the validation data from P_t or the balanced training data, we can estimate the $\hat{\pi}_p = \log \mathbf{q}^*$ as the constrained optimization problem (proof in Section 4.3):

$$\begin{aligned} \mathbf{q}^* &= \underset{\mathbf{q}}{\operatorname{argmin}} \mathcal{R}_t(f_{\text{zs}} - \log \mathbf{q}) \\ \text{s.t. } &\mathbf{q}_i \geq 0, \text{ for } i \in [K], \\ &\sum_{i \in [K]} \mathbf{q}_i = 1. \end{aligned} \quad (3)$$

We constrain the sum of \mathbf{q} to be 1 and ensure that each element is non-negative, guaranteeing that it forms a valid probability distribution. We solve the following Lagrangian problem to find optimal \mathbf{q}^* :

$$\min_{\mathbf{q}} \max_{\lambda_i \geq 0, v} \mathcal{R}_t(f_{\text{zs}} - \log \mathbf{q}) - \sum_i \lambda_i \mathbf{q}_i + v(1 - \sum_{i \in [K]} \mathbf{q}_i) \quad (4)$$

Step 2: GLA ensembling. Given the estimated $\hat{\pi}_p$ and the known downstream training π_s , we ensemble the zero-shot model f_{zs} and the fine-tuned model f_{ft} to get our GLA model f_{gla} via Eq. (2). We can regard $f_{\text{zs}} - \hat{\pi}_p$ and $f_{\text{ft}} - \pi_s$ as the debiased zero-shot model (Figure 2(c)) and debiased fine-tuned models, respectively. Our GLA is actually ensembling two debiased models. Note that, different from [55, 48], we *do not* require a hyper-parameter to adjust the contribution of the two models, the optimal solution is to combine them equally (see Section 4.2 for justification).

4 Theoretical Analysis

In this section, we explain why our GLA model best ensembles the zero-shot and fine-tuned models (Section 4.2) and justify the estimation process of the pre-training label distribution π_p (Section 4.3). We start with some preliminaries on *Bayes* optimal classifier.

4.1 Preliminaries

Suppose we have a pair $(X, Y) \sim P$ takes values in $\mathcal{X} \times \mathcal{Y}$, where Y is the class label of input X .

Definition 2. The 0-1 error (risk) of a classifier $\hat{y} : \mathcal{X} \rightarrow \mathcal{Y}$ on distribution P is given by:

$$\mathcal{R}(\hat{y}) = P(Y \neq \hat{y}(X)) \quad (5)$$

However, the 0-1 error is non-smooth, one typically minimizes a surrogate loss ℓ , e.g., cross-entropy: $\ell(f(\mathbf{x}), y) = \log[\sum_{i \in [K]} \exp(f(\mathbf{x})_i - f(\mathbf{x})_y)]$, where $\hat{y}(\mathbf{x}) = \operatorname{argmax}_i f(\mathbf{x})_i$. It is known that the cross-entropy loss is *Bayes consistent* [53], i.e., a nearly optimal minimizer of the cross-entropy loss ($\mathbb{E}_{\mathbf{x}, y \sim P}[\ell(f(\mathbf{x}), y)]$) is also a nearly optimal optimizer of the mis-classification error ($\mathbb{E}_{\mathbf{x}, y \sim P}[y \neq \hat{y}(\mathbf{x})]$).

Definition 3. The Bayes optimal classifier y^* for P given input \mathbf{x} is defined as:

$$y^*(\mathbf{x}) = \operatorname{argmax}_{y \in \mathcal{Y}} P(y|\mathbf{x}) \quad (6)$$

It is called *Bayes optimal classifier* because on the average *no* other classifier using the same hypothesis and prior knowledge can outperform it.

Lemma 1. The Bayes optimal classifier y^* for P has lower risk than all classifiers $\hat{y} : \mathcal{X} \rightarrow \mathcal{Y}$.

$$\mathcal{R}(y^*) \leq \mathcal{R}(\hat{y}) \quad (7)$$

4.2 Generalized Logit Adjustment Leads to Better Ensembling

Zero-shot and fine-tuned models are complementary. We revisit an empirical phenomena observed in [48] Section 5.1: After exploring a series of measures of diversity, covering predictions and features, they find that zero-shot and fine-tuned models have diverse predictions, despite sharing the same backbone. As the two data distribution P_s and P_p is known to be different, the resulting models leverage different cues to predict: fine-tuned models risk exploiting *spurious correlations and in-domain patterns* which only hold for downstream dataset [46, 3]; On the other hand, zero-shot CLIP models capture *stable correlations* across diverse domains and exhibit much higher robustness [40]. For instance, zero-shot models rely on robust features for decisions that can achieve high performance on sketch and adversarial samples, while the fine-tuned models that trained on real images typically fail on these samples, as they rely on spurious correlations that only hold on real images. We formulate the phenomena in the following assumption.

Assumption 1. Zero-shot and fine-tuned models have diverse predictions:

$$(f_{\text{ft}}(\mathbf{x}) \perp f_{\text{zs}}(\mathbf{x}))|y. \quad (8)$$

We derive the conditional probability $P_t(y|f_{\text{ft}}(\mathbf{x}), f_{\text{zs}}(\mathbf{x}))$ w.r.t. the outputs of $f_{\text{zs}}(\mathbf{x})$ and $f_{\text{ft}}(\mathbf{x})$:

Lemma 2. For a balanced target distribution¹, where $P_t(y) = 1/K$ for all $y \in [K]$, we have:

$$P_t(y|f_{\text{ft}}(\mathbf{x}), f_{\text{zs}}(\mathbf{x})) = \operatorname{softmax}(\underbrace{f_{\text{ft}}(\mathbf{x}) + f_{\text{zs}}(\mathbf{x}) - \pi_s - \pi_p}_{f_{\text{gla}}(\mathbf{x})})(y) \quad (9)$$

Intuitively, since the zero-shot and fine-tuned models provide diverse predictions, conditioned on the two predictions is equivalent to adding the logits in log space. Additionally, as the target distribution is class-balanced, we need to remove the class bias of two models by subtracting π_s and π_p . The formal proof is given in Appendix A.1. Note that the RHS of Eq. (9) is exactly the softmax output of our GLA model by Definition 1, which exhibits the following property:

Proposition 1. Let $g : \mathbb{R}^K \times \mathbb{R}^K \rightarrow \mathbb{R}^K$ be an arbitrary function that ensemble the outputs of f_{zs} and f_{ft} . Our GLA classifier f_{gla} has lower risk than any function $f_g(\mathbf{x}) = g(f_{\text{zs}}(\mathbf{x}), f_{\text{ft}}(\mathbf{x}))$, i.e.

$$\mathcal{R}_t(f_{\text{gla}}) \leq \mathcal{R}_t(f_g). \quad (10)$$

Proof. From Lemma 2 and Definition 1, we have:

$$\operatorname{argmax}_{y \in \mathcal{Y}} f_{\text{gla}}(\mathbf{x})_y = \operatorname{argmax}_{y \in \mathcal{Y}} \operatorname{softmax}(f_{\text{ft}}(\mathbf{x}) + f_{\text{zs}}(\mathbf{x}) - \pi_s - \pi_p)_y = \operatorname{argmax}_{y \in \mathcal{Y}} P_t(y|f_{\text{ft}}(\mathbf{x}), f_{\text{zs}}(\mathbf{x})), \quad (11)$$

which means f_{gla} is the Bayes optimal classifier (see Definition 3) given $f_{\text{ft}}(\mathbf{x})$ and $f_{\text{zs}}(\mathbf{x})$. According to Lemma 1, any other classifier $g(f_{\text{ft}}(\mathbf{x}), f_{\text{zs}}(\mathbf{x}))$ must have higher risk, i.e., $\mathcal{R}_t(f_{\text{gla}}) \leq \mathcal{R}_t(f_g)$. \square

¹This lemma can be easily extended to imbalanced target distributions (proof in Appendix A). Yet, as most test sets are class-balanced, we focus on the balanced case for brevity.

Proposition 1 demonstrates that our f_{gla} model is the *best* model, as it has the lowest risk on target distribution. Proposition 1 further explains the superiority of f_{gla} over the fine-tuned model f_{ft} and the naive ensemble $f_{\text{ens}}(\mathbf{x}) = f_{\text{ft}}(\mathbf{x}) + f_{\text{zs}}(\mathbf{x})$:

Corollary 1. f_{gla} performs better than fine-tuned model f_{ft} and naive emsembling f_{ens} :

$$\mathcal{R}_t(f_{\text{gla}}) \leq \mathcal{R}_t(f_{\text{ft}}), \mathcal{R}_t(f_{\text{gla}}) \leq \mathcal{R}_t(f_{\text{ens}}) \quad (12)$$

Discussion: when do the GLA models degenerate? Note that there are two equality signs in Eq. (12), indicating that the performance of the GLA model can degenerate to be equivalent to that of the fine-tuned model and naive ensembling in the following two cases.

Case 1: For the first equality, if zero-shot model $f_{\text{zs}}(\mathbf{x})$ provides no further information about y given $f_{\text{ft}}(\mathbf{x})$, i.e., $(y \perp f_{\text{zs}}(\mathbf{x}))|f_{\text{ft}}(\mathbf{x})$, then $P_t(y|f_{\text{ft}}(\mathbf{x}), f_{\text{zs}}(\mathbf{x}))$ degenerates to $P_t(y|f_{\text{ft}}(\mathbf{x}))$ and the first equality applies. However, in practice, as downstream model and zero-shot model provides diverse predictions, we usually encounter strict inequality, i.e., $\mathcal{R}_t(f_{\text{gla}}) < \mathcal{R}_t(f_{\text{ft}})$.

Case 2: The second equality applies when pre-training and downstream training distribution are both class-balanced. In fact, the pre-training dataset for foundation models are known to be highly skewed. Therefore, in most cases, we have $\mathcal{R}_t(f_{\text{gla}}) < \mathcal{R}_t(f_{\text{ens}})$.

In summary, the above two equalities are usually unattainable, which means that theoretically, our GLA model performs better than both the fine-tuned and the naive ensemble models.

4.3 Estimate the label bias of the pre-training dataset

However, π_p is usually unknown as we have no access to pre-training dataset. In this work, we seek to estimate π_p using the zero-shot models and the downstream data. Similar to Proposition 1, we have the following proposition says that $f_{\text{zs}} - \pi_p$ has lower error on target distribution than any other classifiers that use f_{zs} , see Appendix A.2 for the full proof.

Proposition 2. Let $h : \mathbb{R}^K \rightarrow \mathbb{R}^K$ be an arbitrary function that predicts labels using the outputs of the zero-shot model $f_{\text{zs}}(\mathbf{x})$. Let the derived classifier be denoted as $f_h(\mathbf{x}) = h(f_{\text{zs}}(\mathbf{x}))$. The classifier $f_{\text{zs}} - \pi_p$ is better than any $f_h(\mathbf{x})$: $\mathcal{R}_t(f_{\text{zs}} - \pi_p) \leq \mathcal{R}_t(f_h(\mathbf{x}))$.

Let \mathbf{q} be an arbitrary probability simplex over K classes, then we have $\mathcal{R}_t(f_{\text{zs}}(\mathbf{x}) - \pi_p) \leq \mathcal{R}_t(f_{\text{zs}}(\mathbf{x}) - \log \mathbf{q})$. Therefore, we choose to optimize a *probability simplex* \mathbf{q} over K classes such that the model $f_{\text{zs}} - \log \mathbf{q}$ achieves the minimal empirical risk, as formulated in Eq. (3) (the Step 1 of GLA algorithm). Once we obtain the estimated class prior $\hat{\pi}_p = \log \mathbf{q}$, we can easily implement the GLA model by ensembling $f_{\text{gla}}(\mathbf{x}) = f_{\text{ft}}(\mathbf{x}) + f_{\text{zs}}(\mathbf{x}) - \pi_s - \hat{\pi}_p$ (the Step 2 of GLA algorithm).

Toy experiment. We conducted an experiment to show that the estimated label distribution closely approximates the true one. Specifically, we trained a model with a ResNet32 backbone on the imbalanced CIFAR-10-LT [10] dataset with an imbalanced ratio of 10. Subsequently, we used only the test set combined with our proposed method to estimate the label distribution. This procedure simulates scenarios where only downstream data is available and the pre-training data is inaccessible.

Figure 3 reveals a strong alignment between the estimated (orange line) and the actual distributions (blue line), which is further emphasized by a small KL-divergence value of 0.00062. The toy experiment validates the effectiveness of our debiasing method.

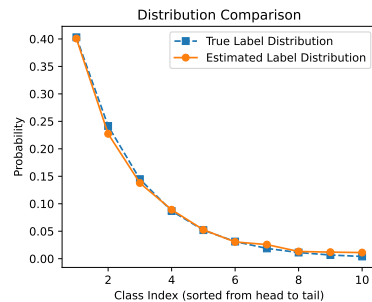


Figure 3: Estimating label bias of CIFAR-10-LT-IB-10.

Discussion. The $\log \mathbf{q}$ we estimated is not the marginal log-probability of the entire pre-training distribution but the label bias matches the downstream distribution. In the above toy experiment, although training and test sets show different label distributions, their conditional distribution $P(\mathbf{x}|y)$ remains invariant. In this case, our estimate will converge to the actual training label bias. For CLIP models, with diverse pre-training data, some might not align with the downstream domain, potentially compromising the accuracy of the estimation of the entire pre-training distribution.

However, we'd like to point out that removing the label bias of entire pre-training distribution may not optimal for downstream tasks. As a thought experiment, consider a pre-training dataset "sketch"

Method	B/32	B/16									
Zero-shot	63.2	68.3	Zero-shot	64.2	67.2	Zero-shot	59.7	64.4	Zero-shot	62.2	64.8
LP	75.8	79.9	LP	80.5	83.1	LP	77.1	83.1	LP	75.6	78.0
E2E	76.3	81.3	E2E	89.4	91.0	E2E	83.7	90.2	E2E	80.0	82.4
WiSE-FT	76.9	81.7	WiSE-FT	90.0	91.3	WiSE-FT	84.5	90.7	WiSE-FT	80.8	82.9
GLA	77.9	82.8	GLA	90.7	91.9	GLA	85.0	91.1	GLA	81.2	83.4

(a) ImageNet

(b) CIFAR100

(c) Stanford Cars

(d) SUN397

Table 1: Accuracy of various methods using CLIP ViT-B/32 and ViT-B/16. LP: linear probe; E2E: end-to-end fine-tuning. Results were obtained using the official implementation from WiSE-FT [48].

and "photo" styles for "dog" and "cat" samples. Suppose the sample size of "dog" and "cat" is equal but there are more "sketch dogs" than "sketch cats". This means that even if the overall distribution is balanced, each style isn't, resulting in biased zero-shot predictions. If we aim to deploy models for the "sketch dogs and cats" domain, adjusting the overall label bias is insufficient. Instead, the optimal label bias should be estimated on the "sketch" distribution. We also provide experiments using LAION-400M dataset in Appendix C.2, illustrating the situation when the downstream data diverges from the pre-training set.

5 Experiments

We evaluate our GLA on three real-world scenarios: many-shot (Section 5.1), few-shot (Section 5.2) and long-tail learning (Section 5.3). We show that our GLA boosts performance on all three settings.

5.1 Many-shot learning

Datasets. We use ImageNet [11] and CIFAR100 [26] for generic object classification, Stanford-Cars [25] for fine-grained classification, and SUN397 [50] for scene recognition. See Appendix B.1 for details.

Baselines. We compare GLA against four methods: (1) Zero-shot model, (2) Linear Probing (LP), (3) End-to-End fine-tuning (E2E), and (4) weight ensembling method WiSE-FT[48].

Implementation details. We consider two models: CLIP ViT-B/32 and ViT-B/16. For learning-based models, we fine-tune with AdamW using a cosine annealing learning rate scheduler. We fine-tune for 10 epochs on ImageNet and 20 epochs on other datasets. See Appendix B.3 for further details.

Main results. Table 1 compares our GLA with various baselines. We observe that our GLA can increase the performance of end-to-end fine-tuned models: it achieves 1.5% gains on ImageNet. Compared to WiSE-FT, GLA gains 1.1% top-1 accuracy boost on ImageNet dataset. Beyond generic object recognition, our method also improves accuracy on the fine-grained dataset (Stanford Cars) and the scene recognition dataset (SUN397), by 0.4% and 0.5%, respectively.

Breakdown performance analysis. To analyze the impact of pre-training label bias on fine-tuned and ensemble models, we present the breakdown results on ImageNet using CLIP ViT-B/16, as shown in Table 2. Specifically, we sort the class index using the estimated π_p , and assign the top third of the classes as the head classes, the last third as the tail classes, and the remaining classes as the medium classes. Due to the label bias, the zero-shot tail performance is significantly lower than the head one (57.2% vs. 78.0%). The resulting E2E models are also affected by the bias, with the tail performance being 6.3% lower than the head. Existing ensemble WiSE-FT overlooks the bias, exhibiting noticeable degradation on the tail performances (-0.9%) compared to E2E model, while our GLA stands out for all three subgroups.

Estimated π_p is transferable across different zero-shot models. The estimated π_p should be transferable across different zero-shot models if they are trained on the same pre-training dataset. To verify this, we employed a CLIP ViT-B/32 based zero-shot model to estimate π_p , which is subsequently used to debias zero-shot models based on CLIP ViT-B/16 and ViT-L/14. As shown in Table 3, our debiased models outperform the original zero-shot versions by a clear margin.

Method	Head	Med.	Tail	All
Zero-shot	78.0	69.8	57.2	68.3
E2E	83.6	83.0	77.3	81.3
WiSE-FT	85.3	83.7	76.4	81.7
GLA	85.2	84.3	78.8	82.8

Table 2: Breakdown results on ImageNet.

Model	Source	Target	
	ViT-B/32	ViT-B/16	ViT-L/14
$f_{zs}(\mathbf{x})$	63.4	68.8	75.6
$f_{zs}(\mathbf{x}) - \hat{\pi}_p$	65.4	69.3	76.3

Table 3: Estimated $\hat{\pi}_p$ is transferable across different backbones. $\hat{\pi}_p$ is estimated using CLIP ViT-B/32.

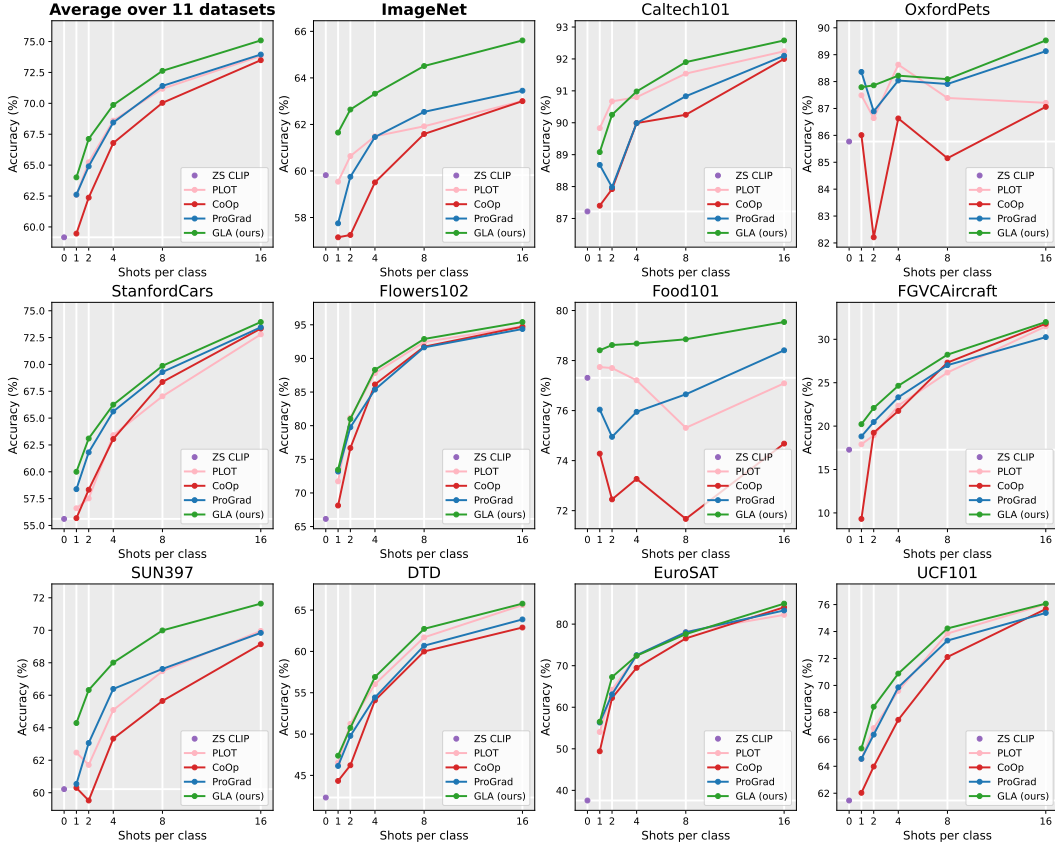


Figure 5: Accuracy (%) of few-shot learning on 11 datasets.

Ensembling with mixing coefficient. In Section 5.1, we prove the optimal solution is to combine the debiased zero-shot and fine-tuned models equally. We now examine the claim by introducing a mixture coefficient $\alpha \in [0, 1]$. The ensemble predictions are given by: $f_{gla}(\mathbf{x}, \alpha) = (1 - \alpha) \cdot (f_{zs}(\mathbf{x}) - \pi_p) + \alpha \cdot (f_{ft}(\mathbf{x}) - \pi_s)$. We compare the GLA and the naive ensembling with mixture α in Figure 4, where GLA meets its optimal performance at $\alpha = 0.5$, which is in line with our theoretical analysis. We also observe that the debiased zero-shot model increases accuracy by 2.3% and our GLA consistently outperforms naive ensembling with various α .

5.2 Few-shot learning

For few-shot scenarios, we primarily choose prompt tuning for fine-tuning, since it is empirically more effective than end-to-end fine-tuning and linear probing [54, 55, 8].

Datasets. We follow CoOp[54] to use 15 datasets: ImageNet [11], Caltech101 [13], OxfordPets [37], StanfordCars [25], Flowers102 [36], Food101 [6], FGVCaircraft [34], EuroSAT [16], UCF101 [44],

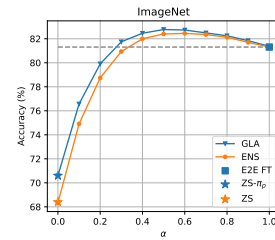


Figure 4: Accuracy with mixing coefficient α .

Method	Source	Target			
	IN	V2	S	A	R
CLIP	59.8	52.8	35.5	22.8	60.6
CoOp	61.9	54.3	32.5	21.8	54.2
PLOT	63.0	55.1	33.0	21.9	55.6
ProGrad	63.5	55.4	33.1	21.3	55.2
GLA	65.6	57.1	36.4	23.0	62.1

Table 4: Evaluation on robustness to distribution shift at 16 training shots.

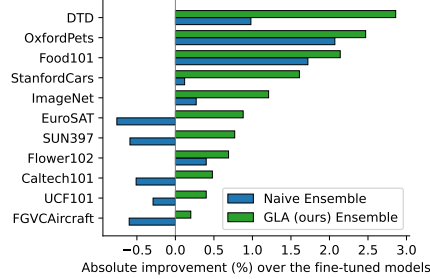


Figure 6: Comparison with naive ensembling.

Model	IN.	Caltech.	Pets.	Cars.	Flowers.	Food.	Aircraft.	SUN.	DTD	EuroSAT	UCF.	Avg.
f_{zs}	59.8	87.1	85.8	55.6	65.3	77.9	17.1	60.3	42.3	37.5	61.5	59.1
$f_{zs} - \hat{\pi}_p$	62.3	89.9	85.9	57.6	67.2	78.6	18.4	63.5	43.0	39.0	62.4	60.7
Δ	+2.5	+2.7	+0.1	+2.0	+1.9	+0.7	+1.3	+3.2	+0.7	+1.4	+0.9	+1.6

Table 5: Comparison between zero-shot models (f_{zs}) and debiased zero-shot models ($f_{zs} - \hat{\pi}_p$).

DTD [9], SUN397 [50], ImageNet-{V2 [41], Sketch [47], A [18], R [17]}. We randomly select {1, 2, 4, 8, 16} shots for training and use the original test set for evaluation. See Appendix B.1 for details.

Baselines. We compare with three prompt tuning methods: (1) CoOp [54] optimizes prompts via empirical risk minimization; (2) ProGrad [55] prevents forgetting the general knowledge using zero-shot predictions; (3) PLOT [8] applies optimal transport to match the vision and text modalities.

Implementation details. We implement our proposed GLA method using CLIP-ResNet-50 as the foundation model and adopt class-specific prompt tuning from CoOp. Results are averaged over three seeds, with training configurations aligned with CoOp. See Appendix B.4 for further information.

Main results. Figure 5 summarizes the few-shot results on 11 datasets. The detailed accuracy and standard deviation are in Appendix C.1. Overall, our GLA clearly outperforms the baselines on average performance by a large margin, *e.g.*, our GLA gains 4.6%, 4.8%, 3.1%, 2.6% and 1.6% performance boost over CoOp at 1, 2, 4, 8, 16 shots. In particular, on ImageNet dataset, we observe a large improvement, *e.g.*, 3.9%, 2.9%, 1.9%, 2.0% and 2.2% over ProGrad at 1, 2, 4, 8, 16 shots. Furthermore, on OxfordPerts, Food101 and SUN397 datasets, our method’s performance remains stable and consistently improves with increasing sample sizes, while the one of the baseline methods fluctuates significantly. In particular, on Food101, baseline models even underperform zero-shot models by a large margin, while our GLA shows clearly better performance than zero-shot models.

Robustness to distribution shifts. Following CoOp, we used the ImageNet at 16 training shots as the source domain and assess the robustness on ImageNet-{V2, Sketch, A, R} datasets. Table 4 summarizes the results, where the prompt tuning baselines perform worse on distribution shifted datasets compared to the zero-shot model, as fine-tuning on limited data misleads the model to learn in-distribution correlations. In comparison, our GLA approach makes the best of both fine-tuned and zero-shot models, thus consistently outperforms other methods on both source and target domains.

GLA improves accuracy over naive ensemble. Figure 6 compares the results between our GLA and naive ensembling. We rank the absolute improvements over fine-tuning baseline at 16 training shots. In summary, our GLA demonstrates superior accuracy gains. It is worth noting that the naive ensembling does not always lead to improvements, *e.g.*, on EuroSAT, SUN, Caltech, UCF and Aircraft, naive ensembling even underperforms fine-tuning baseline.

Debiased zero-shot models perform better. We estimate π_p at 16 shots and compare the original zero-shot models with the debiased zero-shot models in Table 5. It is clear that the debiasing leads to improvement on all 11 datasets, showcasing an average accuracy gain of 1.6%.

5.3 Long-tail learning

Datasets and metrics. We evaluate our method on two standard benchmarks: Places365-LT and ImageNet-LT [31]. In addition to top-1 accuracy, we report the accuracy on three test subsets

	Method	Many	Med	Few	All		Method	Many	Med	Few	All
LP	ERM	64.4	39.8	20.1	46.6	LP	ERM	43.9	21.1	9.0	26.9
	LA	56.7	50.5	46.4	52.3		LA	39.2	33.7	29.5	34.9
	BS	57.7	50.5	43.9	52.4		BS	39.6	34.0	28.3	34.9
	GLA	65.5	60.8	57.7	62.2		GLA	43.6	40.2	38.8	41.1
PT	ERM	66.6	57.7	53.8	60.6	PT	ERM	47.7	32.6	24.9	36.5
	LA	67.9	60.0	58.7	62.9		LA	43.9	40.6	39.4	41.5
	BS	67.0	62.2	59.4	63.5		BS	43.4	42.5	42.3	42.8
	GLA	70.7	66.5	64.3	67.8		GLA	47.0	47.1	47.8	47.2
E2E	ERM	75.5	56.0	36.2	60.8	E2E	ERM	46.3	27.4	12.5	31.3
	LWS [24]	70.4	62.6	56.2	64.7		LWS [24]	41.2	39.0	32.8	38.6
	LA [35]	70.4	62.8	56.9	64.9		LA [35]	42.2	39.3	34.0	39.3
	BS [43]	71.2	62.5	56.8	65.1		BS [43]	46.7	44.4	39.5	44.3
	WiSE-FT [48]	70.7	65.0	61.1	66.7		WiSE-FT [48]	46.0	44.0	43.9	44.7
	BALLAD [33]	71.0	66.3	59.5	67.2		BALLAD [33]	48.7	44.7	42.2	45.7
	GLA	72.1	66.4	63.4	68.2		GLA	47.3	45.4	45.3	46.1

(a) ImageNet-LT

(b) Places365-LT

Table 6: The performances on ImageNet-LT and Places365-LT.

according to the number of samples per class: many-shot (> 100 samples), medium-shot ($20 \sim 100$ samples), and few-shot (< 20 samples). Detailed information is provided in Appendix B.1.

Fine-tuning and long-tail learning baselines. We compare our GLA with the combinations of fine-tuning protocols and long-tailed recognition methods. We consider three fine-tuning protocols: 1) Linear Probe (LP) 2) End-to-End (E2E) fine-tuning; 3) Prompt Tuning (PT). The three fine-tuning paradigms are introduced in Section 3.1 with details in Appendix B.3. We compare with 5 long-tail learning methods: 1) standard Empirical Risk Minimization (ERM); 2) Learnable Weight Scaling (LWS) [24]; 3) Logit Adjustment (LA) [35]; 4) Balanced Softmax (BS) [43], and 5) BALLAD [33], which is designed for VLMs. See Appendix B.6 for more details on long-tail baselines.

Implementation Details. For all combinations of the fine-tuning and long-tail learning baselines, visual backbones are initialized from CLIP-ResNet-50 and classifiers are initialized via zero-shot prompting. We use SGD for 50 epochs with batch size of 512. See Appendix B.6 for further details.

Results. Table 6 shows that our GLA method consistently surpasses baselines across all long-tailed datasets. Our approach outperforms PT-based models by 3.5% and 4.4% on ImageNet-LT and Places365-LT, respectively. Against E2E approaches, GLA exceeds not just the WiSE-FT but also the current SOTA method BALLAD, by a large margin, *e.g.*, 1pp gains on ImageNet-LT.

6 Conclusion and Limitation

In this paper, we identify the label bias in foundation models and underscore its adverse effects on downstream task performance. We propose the Generalized Logit Adjustment (GLA) framework for fine-tuning foundation models, which boosts the performance by effectively eliminating label bias and combining diverse predictions from zero-shot and fine-tuned models. We prove that when presented with zero-shot and fine-tuned models, our GLA is the Bayes optimal classifier for downstream task. Extensive experiments across a diverse range of tasks and fine-tuning framework demonstrate the effectiveness of our approach. We believe that the proposed GLA may partially improve the fairness and credibility of foundation models.

The first limitation is that we only focus on the label bias while other forms of model biases, *e.g.*, representation bias [5], cannot be addressed by our algorithm yet. The second limitation is that we primarily focus on enhancing the fine-tuning performance for discriminative models. However, applying our GLA framework to generative models presents challenges. For instance, language generation operates as a Markov process, meaning each output depends on previous ones. This implies it’s not straightforward to estimate the biasedness of a sequence with our GLA, as we only compute the bias in a pre-defined and independent label space.

Acknowledgments

This research is supported by the National Research Foundation, Singapore under its AI Singapore Programme (AISG Award No: AISG2-PhD-2021-01-002 and AI Singapore AISG2-RP-2021-022).

References

- [1] Jean-Baptiste Alayrac, Jeff Donahue, Pauline Luc, Antoine Miech, Iain Barr, Yana Hasson, Karel Lenc, Arthur Mensch, Katherine Millican, Malcolm Reynolds, et al. Flamingo: a visual language model for few-shot learning. *NeurIPS*, 2022.
- [2] James Urquhart Allingham, Jie Ren, Michael W Dusenberry, Xiuye Gu, Yin Cui, Dustin Tran, Jeremiah Zhe Liu, and Balaji Lakshminarayanan. A simple zero-shot prompt weighting technique to improve prompt ensembling in text-image models. In *ICML*, 2023.
- [3] Martin Arjovsky. *Out of distribution generalization in machine learning*. PhD thesis, New York University, 2020.
- [4] Eric Bauer and Ron Kohavi. An empirical comparison of voting classification algorithms: Bagging, boosting, and variants. *Machine learning*, 1999.
- [5] Rishi Bommasani, Drew A Hudson, Ehsan Adeli, Russ Altman, Simran Arora, Sydney von Arx, Michael S Bernstein, Jeannette Bohg, Antoine Bosselut, Emma Brunskill, et al. On the opportunities and risks of foundation models. *Technical Report*, 2021.
- [6] Lukas Bossard, Matthieu Guillaumin, and Luc Van Gool. Food-101—mining discriminative components with random forests. In *ECCV*, 2014.
- [7] Tom B. Brown, Benjamin Mann, Nick Ryder, Melanie Subbiah, Jared Kaplan, Prafulla Dhariwal, Arvind Neelakantan, Pranav Shyam, Girish Sastry, Amanda Askell, Sandhini Agarwal, Ariel Herbert-Voss, Gretchen Krueger, Tom Henighan, Rewon Child, Aditya Ramesh, Daniel M. Ziegler, Jeffrey Wu, Clemens Winter, Christopher Hesse, Mark Chen, Eric Sigler, Mateusz Litwin, Scott Gray, Benjamin Chess, Jack Clark, Christopher Berner, Sam McCandlish, Alec Radford, Ilya Sutskever, and Dario Amodei. Language models are few-shot learners. In *NeurIPS*, 2020.
- [8] Guangyi Chen, Weiran Yao, Xiangchen Song, Xinyue Li, Yongming Rao, and Kun Zhang. Prompt learning with optimal transport for vision-language models. *ICLR*, 2023.
- [9] Mircea Cimpoi, Subhransu Maji, Iasonas Kokkinos, Sammy Mohamed, and Andrea Vedaldi. Describing textures in the wild. In *CVPR*, 2014.
- [10] Yin Cui, Menglin Jia, Tsung-Yi Lin, Yang Song, and Serge Belongie. Class-balanced loss based on effective number of samples. In *CVPR*, 2019.
- [11] Jia Deng, Wei Dong, Richard Socher, Li-Jia Li, Kai Li, and Li Fei-Fei. Imagenet: A large-scale hierarchical image database. In *CVPR*, 2009.
- [12] Thomas G Dietterich. Ensemble methods in machine learning. In *Multiple Classifier Systems: First International Workshop*, 2000.
- [13] Li Fei-Fei, Rob Fergus, and Pietro Perona. Learning generative visual models from few training examples: An incremental bayesian approach tested on 101 object categories. In *CVPRW*, 2004.
- [14] Yoav Freund and Robert E Schapire. A decision-theoretic generalization of on-line learning and an application to boosting. *Journal of computer and system sciences*, 1997.
- [15] Jose Gallego-Posada and Juan Ramirez. Cooper: a toolkit for Lagrangian-based constrained optimization. <https://github.com/cooper-org/cooper>, 2022.
- [16] Patrick Helber, Benjamin Bischke, Andreas Dengel, and Damian Borth. Eurosat: A novel dataset and deep learning benchmark for land use and land cover classification. *IEEE Journal of Selected Topics in Applied Earth Observations and Remote Sensing*, 2019.

- [17] Dan Hendrycks, Steven Basart, Norman Mu, Saurav Kadavath, Frank Wang, Evan Dorundo, Rahul Desai, Tyler Zhu, Samyak Parajuli, Mike Guo, et al. The many faces of robustness: A critical analysis of out-of-distribution generalization. In *CVPR*, 2021.
- [18] Dan Hendrycks, Kevin Zhao, Steven Basart, Jacob Steinhardt, and Dawn Song. Natural adversarial examples. In *CVPR*, 2021.
- [19] Geoffrey Hinton, Oriol Vinyals, and Jeff Dean. Distilling the knowledge in a neural network. *NeurIPS Workshop*, 2014.
- [20] Youngkyu Hong, Seungju Han, Kwanghee Choi, Seokjun Seo, Beomsu Kim, and Buru Chang. Disentangling label distribution for long-tailed visual recognition. In *CVPR*, 2021.
- [21] Gabriel Ilharco, Mitchell Wortsman, Ross Wightman, Cade Gordon, Nicholas Carlini, Rohan Taori, Achal Dave, Vaishaal Shankar, Hongseok Namkoong, John Miller, Hannaneh Hajishirzi, Ali Farhadi, and Ludwig Schmidt. Openclip. Technical report, Zenodo, jul 2021.
- [22] Pavel Izmailov, Dmitrii Podoprikin, Timur Garipov, Dmitry Vetrov, and Andrew Gordon Wilson. Averaging weights leads to wider optima and better generalization. *UAI*, 2018.
- [23] Chao Jia, Yinfei Yang, Ye Xia, Yi-Ting Chen, Zarana Parekh, Hieu Pham, Quoc Le, Yun-Hsuan Sung, Zhen Li, and Tom Duerig. Scaling up visual and vision-language representation learning with noisy text supervision. In *ICML*, 2021.
- [24] Bingyi Kang, Saining Xie, Marcus Rohrbach, Zhicheng Yan, Albert Gordo, Jiashi Feng, and Yannis Kalantidis. Decoupling representation and classifier for long-tailed recognition. In *ICLR*, 2020.
- [25] Jonathan Krause, Michael Stark, Jia Deng, and Li Fei-Fei. 3d object representations for fine-grained categorization. In *CVPRW*, 2013.
- [26] Alex Krizhevsky. Learning multiple layers of features from tiny images. Technical report, University of Toronto, 2009.
- [27] Ananya Kumar, Tengyu Ma, Percy Liang, and Aditi Raghunathan. Calibrated ensembles can mitigate accuracy tradeoffs under distribution shift. In *UAI*. PMLR, 2022.
- [28] Balaji Lakshminarayanan, Alexander Pritzel, and Charles Blundell. Simple and scalable predictive uncertainty estimation using deep ensembles. *NeurIPS*, 2017.
- [29] Tao Lin, Lingjing Kong, Sebastian U Stich, and Martin Jaggi. Ensemble distillation for robust model fusion in federated learning. In H. Larochelle, M. Ranzato, R. Hadsell, M.F. Balcan, and H. Lin, editors, *NeurIPS*, 2020.
- [30] Zachary Lipton, Yu-Xiang Wang, and Alexander Smola. Detecting and correcting for label shift with black box predictors. In *ICML*, 2018.
- [31] Ziwei Liu, Zhongqi Miao, Xiaohang Zhan, Jiayun Wang, Boqing Gong, and Stella X Yu. Large-scale long-tailed recognition in an open world. In *CVPR*, 2019.
- [32] Ilya Loshchilov and Frank Hutter. Decoupled weight decay regularization. In *ICLR*, 2019.
- [33] Teli Ma, Shijie Geng, Mengmeng Wang, Jing Shao, Jiasen Lu, Hongsheng Li, Peng Gao, and Yu Qiao. A simple long-tailed recognition baseline via vision-language model. *arXiv preprint arXiv:2111.14745*, 2021.
- [34] Subhransu Maji, Esa Rahtu, Juho Kannala, Matthew Blaschko, and Andrea Vedaldi. Fine-grained visual classification of aircraft. *arXiv preprint arXiv:1306.5151*, 2013.
- [35] Aditya Krishna Menon, Sadeep Jayasumana, Ankit Singh Rawat, Himanshu Jain, Andreas Veit, and Sanjiv Kumar. Long-tail learning via logit adjustment. In *ICLR*, 2021.
- [36] Maria-Elena Nilsback and Andrew Zisserman. Automated flower classification over a large number of classes. In *Indian Conference on Computer Vision, Graphics & Image Processing*, 2008.

- [37] Omkar M Parkhi, Andrea Vedaldi, Andrew Zisserman, and CV Jawahar. Cats and dogs. In *CVPR*, 2012.
- [38] Xingchao Peng, Qinxun Bai, Xide Xia, Zijun Huang, Kate Saenko, and Bo Wang. Moment matching for multi-source domain adaptation. In *ICCV*, 2019.
- [39] Hieu Pham, Zihang Dai, Golnaz Ghiasi, Kenji Kawaguchi, Hanxiao Liu, Adams Wei Yu, Jiahui Yu, Yi-Ting Chen, Minh-Thang Luong, Yonghui Wu, et al. Combined scaling for zero-shot transfer learning. *arXiv preprint arXiv:2111.10050*, 2021.
- [40] Alec Radford, Jong Wook Kim, Chris Hallacy, Aditya Ramesh, Gabriel Goh, Sandhini Agarwal, Girish Sastry, Amanda Askell, Pamela Mishkin, Jack Clark, et al. Learning transferable visual models from natural language supervision. In *ICML*, 2021.
- [41] Benjamin Recht, Rebecca Roelofs, Ludwig Schmidt, and Vaishaal Shankar. Do imagenet classifiers generalize to imagenet? In *ICML*, 2019.
- [42] William J Reed. The pareto, zipf and other power laws. *Economics letters*, 2001.
- [43] Jiawei Ren, Cunjun Yu, Xiao Ma, Haiyu Zhao, Shuai Yi, et al. Balanced meta-softmax for long-tailed visual recognition. *NeurIPS*, 2020.
- [44] Khurram Soomro, Amir Roshan Zamir, and Mubarak Shah. Ucf101: A dataset of 101 human actions classes from videos in the wild. *arXiv preprint arXiv:1212.0402*, 2012.
- [45] Kaihua Tang, Jianqiang Huang, and Hanwang Zhang. Long-tailed classification by keeping the good and removing the bad momentum causal effect. *NeurIPS*, 2020.
- [46] Rohan Taori, Achal Dave, Vaishaal Shankar, Nicholas Carlini, Benjamin Recht, and Ludwig Schmidt. Measuring robustness to natural distribution shifts in image classification. *NeurIPS*, 2020.
- [47] Haohan Wang, Songwei Ge, Zachary Lipton, and Eric P Xing. Learning robust global representations by penalizing local predictive power. *NeurIPS*, 2019.
- [48] Mitchell Wortsman, Gabriel Ilharco, Jong Wook Kim, Mike Li, Simon Kornblith, Rebecca Roelofs, Raphael Gontijo Lopes, Hannaneh Hajishirzi, Ali Farhadi, Hongseok Namkoong, et al. Robust fine-tuning of zero-shot models. In *CVPR*, 2022. <https://arxiv.org/abs/2109.01903>.
- [49] Tong Wu, Ziwei Liu, Qingqiu Huang, Yu Wang, and Dahua Lin. Adversarial robustness under long-tailed distribution. *CVPR*, 2021.
- [50] Jianxiong Xiao, James Hays, Krista A Ehinger, Aude Oliva, and Antonio Torralba. Sun database: Large-scale scene recognition from abbey to zoo. In *CVPR*, 2010.
- [51] Xuanyu Yi, Jiajun Deng, Qianru Sun, Xian-Sheng Hua, Joo-Hwee Lim, and Hanwang Zhang. Invariant training 2d-3d joint hard samples for few-shot point cloud recognition. In *ICCV*, 2023.
- [52] Jiahui Yu, Zirui Wang, Vijay Vasudevan, Legg Yeung, Mojtaba Seyedhosseini, and Yonghui Wu. Coca: Contrastive captioners are image-text foundation models. *TMLR*, 2022.
- [53] Tong Zhang. Statistical behavior and consistency of classification methods based on convex risk minimization. *The Annals of Statistics*, 2004.
- [54] Kaiyang Zhou, Jingkang Yang, Chen Change Loy, and Ziwei Liu. Learning to prompt for vision-language models. *IJCV*, 2022.
- [55] Beier Zhu, Yulei Niu, Yucheng Han, Yue Wu, and Hanwang Zhang. Prompt-aligned gradient for prompt tuning. In *ICCV*, 2023.
- [56] Beier Zhu, Yulei Niu, Saeil Lee, Minhoe Hur, and Hanwang Zhang. Debaised fine-tuning for vision-language models by prompt regularization. *AAAI*, 2023.

A Proofs

A.1 Proof of Lemma 2

Restated Lemma (Lemma 2). Let π_t denote the log probability of the target label distribution $\pi_t(y) = \log P_t(y)$, we have:

$$P_t(y|f_{ft}(\mathbf{x}), f_{zs}(\mathbf{x})) = \text{softmax}(f_{ft}(\mathbf{x}) + f_{zs}(\mathbf{x}) - \pi_s - \pi_p + \pi_t)(y). \quad (13)$$

In class-balanced target distribution, Eq. (13) simplifies to:

$$P_t(y|f_{ft}(\mathbf{x}), f_{zs}(\mathbf{x})) = \text{softmax}(f_{ft}(\mathbf{x}) + f_{zs}(\mathbf{x}) - \pi_s - \pi_p)(y). \quad (14)$$

Proof. Denote the output $\mathbf{e} = f_{ft}(\mathbf{x})$ and $\mathbf{z} = f_{zs}(\mathbf{x})$. We first use the Bayes Rule to decompose $P_t(y|\mathbf{e}, \mathbf{z})$ into $P_t(\mathbf{e}, \mathbf{z}|y)$, $P_t(y)$ and $P_t(\mathbf{e}, \mathbf{z})$ in Eq. (15), then rewrite $P_t(\mathbf{e}, \mathbf{z}|y)$ in Eq. (16) according to Assumption 1. Focusing on label shift problem [35, 20, 30] where $P(\mathbf{x}|y)$ does not change, we derive Eq. (17)

$$P_t(y|\mathbf{e}, \mathbf{z}) = \frac{P_t(\mathbf{e}, \mathbf{z}|y)P_t(y)}{P_t(\mathbf{e}, \mathbf{z})} \quad (15)$$

$$= P_t(\mathbf{e}|y)P_t(\mathbf{z}|y)\frac{P_t(y)}{P_t(\mathbf{e}, \mathbf{z})} \quad (16)$$

$$= P_s(\mathbf{e}|y)P_p(\mathbf{z}|y)\frac{P_t(y)}{P_t(\mathbf{e}, \mathbf{z})} \quad (17)$$

$$= \frac{P_s(y|\mathbf{e})P_s(\mathbf{e})}{P_s(y)} \frac{P_p(y|\mathbf{z})P_p(\mathbf{z})}{P_p(y)} \frac{P_t(y)}{P_t(\mathbf{e}, \mathbf{z})} \quad (18)$$

$$= \frac{P_s(y|\mathbf{e})}{P_s(y)} \frac{P_p(y|\mathbf{z})}{P_p(y)} \frac{P_s(\mathbf{e})P_p(\mathbf{z})P_t(y)}{P_t(\mathbf{e}, \mathbf{z})} \quad (19)$$

$$(20)$$

Since \mathbf{e}, \mathbf{z} are fixed, we can replace the terms that not rely on y with a constant C_1 in Eq. (21). We replace $P_s(y) = \exp(\log P_s(y)) = \exp(\pi_s(y))$, $P_p(y) = \exp(\log P_p(y)) = \exp(\pi_p(y))$ and $P_t(y) = \exp(\log P_t(y)) = \exp(\pi_t(y))$. Suppose the underlying class-probabilities $P_s(y|\mathbf{e}) \propto \exp(\mathbf{e}_y)$ and $P_p(y|\mathbf{z}) \propto \exp(\mathbf{z}_y)$ for $y \in [K]$. Denote the constants C_s and C_p for normalizing $\exp(\mathbf{e}_y)$ and $\exp(\mathbf{z}_y)$ into probabilities, and merge all constants to $C = \frac{C_1}{C_s C_p}$, we get Eq. (23)

$$P_t(y|\mathbf{e}, \mathbf{z}) = \frac{P_s(y|\mathbf{e})}{P_s(y)} \frac{P_p(y|\mathbf{z})}{P_p(y)} P_t(y) C_1 \quad (21)$$

$$= \exp(\mathbf{e} + \mathbf{z} - \pi_s - \pi_p + \pi_t)(y) \frac{C_1}{C_s C_p} \quad (22)$$

$$= C \cdot \exp(\mathbf{e} + \mathbf{z} - \pi_s - \pi_p + \pi_t)(y) \quad (23)$$

Because the summation of $P_t(y|\mathbf{e}, \mathbf{z})$ is 1, $C = 1 / \sum_{i \in [K]} \exp(\mathbf{e} + \mathbf{z} - \pi_s - \pi_p + \pi_t)(i)$. Therefore, we have:

$$P_t(y|f_{ft}(\mathbf{x}), f_{zs}(\mathbf{x})) = P_t(y|\mathbf{e}, \mathbf{z}) \quad (24)$$

$$= \frac{\exp(\mathbf{e} + \mathbf{z} - \pi_s - \pi_p)_y}{\sum_{i \in [K]} \exp(\mathbf{e} + \mathbf{z} - \pi_s - \pi_p + \pi_t)_i} \quad (25)$$

$$= \text{softmax}(f_{ft}(\mathbf{x}) + f_{zs}(\mathbf{x}) - \pi_s - \pi_p + \pi_t)_y \quad (26)$$

In class-balanced target distribution case, $\pi_t = \log \frac{1}{K}$ is constant. Since the softmax function is invariant to constant offsets, Eq. (26) simplifies to:

$$P_t(y|f_{ft}(\mathbf{x}), f_{zs}(\mathbf{x})) = \text{softmax}(f_{ft}(\mathbf{x}) + f_{zs}(\mathbf{x}) - \pi_s - \pi_p)_y \quad (27)$$

□

Dataset	Classes	Train size	Test size	Task
ImageNet	1,000	1.28M	50,000	Object-level
CIFAR100	100	50,000	10,000	Object-level
Caltech101	100	4,128	2,465	Object-level
DTD	47	2,820	1,692	Textures
EuroSAT	10	13,500	8,100	Satellite images
FGVCAircraft	100	3,334	3,333	Fine-grained aircraft
Flowers102	102	4,093	2,463	Fine-grained flowers
Food101	101	50,500	30,300	Fine-grained food
OxfordPets	37	2,944	3,669	Fine-grained pets
StanfordCars	196	6,509	8,041	Fine-grained car
SUN397	397	15,880	19,850	Scene-level
UCF101	101	7,639	3,783	Action
ImageNetV2	1,000	-	10,000	Robustness to collocation
ImageNet-Sketch	1000	-	50,889	Robustness to sketch domain
ImageNet-A	200	-	7,500	Robustness to adversarial attack
ImageNet-R	200	-	30,000	Robustness to multi-domains

Table 7: The detailed statistics of datasets for many-shot and few-shot learning.

A.2 Proof of Proposition 2

Restated Proposition (Proposition 2). *Suppose that the target distribution P_p is class-balanced. Let $h : \mathbb{R}^K \rightarrow \mathbb{R}^K$ be an arbitrary function that predicts labels using the outputs of the zero-shot model $f_{zs}(\mathbf{x})$. Let the derived classifier be denoted as $f_h(\mathbf{x}) = h(f_{zs}(\mathbf{x}))$. The classifier $f_{zs} - \pi_p$ is better than any $f_h(\mathbf{x})$: $\mathcal{R}_t(f_{zs} - \pi_p) \leq \mathcal{R}_t(f_h(\mathbf{x}))$.*

Proof. Denote the output $\mathbf{z} = f_{zs}(\mathbf{x})$. Similar to Eq. (15)-Eq. (26), we have

$$P_t(y|\mathbf{z}) = \frac{P_t(\mathbf{z}|y)P_t(y)}{P_t(\mathbf{z})} \quad (28)$$

$$= \frac{P_p(\mathbf{z}|y)P_t(y)}{P_t(\mathbf{z})} \quad (29)$$

$$= \frac{P_p(y|\mathbf{z})P_t(y)}{P_p(y)P_t(\mathbf{z})} \quad (30)$$

$$= \exp(\mathbf{z} - \pi_p)(y) / \sum_{i \in [K]} \exp((\mathbf{z} - \pi_p)(i)) \quad (31)$$

$$= \text{softmax}(\mathbf{z} - \pi_p) = \text{softmax}(f_{zs}(\mathbf{x}) - \pi_p) \quad (32)$$

Therefore, we have:

$$\operatorname{argmax}_{y \in \mathcal{Y}} (f_{zs}(\mathbf{x}) - \pi_p)_y = \operatorname{argmax}_{y \in \mathcal{Y}} \text{softmax}(f_{zs}(\mathbf{x}) - \pi_p)_y = \operatorname{argmax}_{y \in \mathcal{Y}} P_t(y|f_{zs}(\mathbf{x})) \quad (33)$$

Again, using Lemma 1, any other classifier $f_h(\mathbf{x})$ has higher risk than $f_{zs}(\mathbf{x}) - \pi_p$, i.e., $\mathcal{R}_t(f_{zs} - \pi_p) \leq \mathcal{R}_t(f_h(\mathbf{x}))$. \square

B Experimental Details

B.1 Dataset details

Many-shot and few-shot datasets. For many-shot learning, we use ImageNet, CIFAR100, Stanford-Cars and SUN397 datasets. For few-shot learning, we evaluate models on 15 datasets. The details of each dataset are presented in Table 7.

Long-tail datasets. We use two standard long-tail benchmarks: Places365-LT and ImageNet-LT [31]. The skewness of a long-tailed training set is typically represented by imbalanced ratio, which is defined as N_{\max}/N_{\min} . N_{\max} (N_{\min}) denotes the largest (smallest) number of instances per class. A

Dataset	Size of all classes	Size of many classes	Size of medium classes	Size of few classes	Size of training samples	Imbalanced ratio
Places365-LT	365	131	163	71	62.5K	996
ImageNet-LT	1000	385	479	136	186K	256

Table 8: Details of long-tailed datasets.

larger imbalanced ratio means a more imbalanced training set. The test sets are divided into three splits: many-shot subset contains classes with > 100 images, medium-shot subset includes classes with ≥ 20 & ≤ 100 images, and few-shot subset covers classes with < 20 images. Details are listed in Table 8.

B.2 CLIP zero-shot

We use prompt ensembling of 80 prompts provided by CLIP [48] for ImageNet, CIFAR100, and Caltech101 to improve performance, *i.e.*, averaging the text embedding of many captions, *e.g.*, “a photo of a $\{c_k\}$.” and “an image of a $\{c_k\}$.”. For OxfordPets, StanfordCars, Flowers102, Food101, FGV-CAircraft, EuroSAT, UCF101, DTD and SUN397, we use the pre-defined prompt from CoOp [54].

B.3 Fine-tuned models

End-to-end and linear probe fine-tuning. We follow WiSE-FT [48] to implement fine-tuning. We initialize the classifier with the zero-shot classifier and the output of the image encoder Φ_v is normalized during fine-tuning. We fine-tune for a total of 10 epochs using AdamW [32] optimizer with default hyper-parameters $\beta_1 = 0.9, \beta_2 = 0.999, \epsilon = 10^{-8}$ and weight decay 0.1. We choose a batch size of 512. We use the same data augmentation and cosine-annealing learning rate schedule as [48].

B.4 Prompt tuning.

Prompt tuning like CoOp [54] automates prompt engineering by learning the prompt given few samples from downstream tasks. CoOp provides two options of prompt design: unified prompt that is shared among all classes and class-specific prompt that is different for each class. In this paper, we adopt the class-specific prompt design as the fine-tuned model to implement GLA. In specific, given the word embedding \mathbf{t}_k^0 initialized by zero-shot prompts, we aim to learn a collection of class-specific word embedding $\mathbf{R} = \{\mathbf{r}_k\}_{k=1}^K$, such that the text input $\mathbf{t}_k = \mathbf{t}_k^0 + \mathbf{r}_k$ minimizes the empirical risk: $\mathbf{R}^* = \arg\min_{\mathbf{R}} \mathbb{E}_{\mathbf{x}, y} [y \neq \arg\max_i f(x; \mathbf{R})_i]$.

We adhere CoOp to use CLIP ResNet-50 as image encoder for few-shot classification. The word embedding \mathbf{R} is initialized from zeros. For the m few-shot classification setting (where $m \in \{1, 2, 4, 8, 16\}$), we randomly sample m training and m validation points from the respective full datasets. For all few-shot datasets except ImageNet, the training epoch is set to 200 for 16/8 shots, 100 for 4/2 shots, and 50 for 1 shot. For ImageNet, the epoch is set to 50 for all shots. We fine-tune the prompt with SGD optimizer decayed by the cosine annealing rule. The base initial learning rate and batch size are set to 10^{-4} and 32. When given an m -shot sample setting, we increase the learning rate and batch size by m times simultaneously to accelerate the training speed.

B.5 Estimation of the class prior

To estimate the log-probability of the pre-training distribution $\hat{\pi}_s = \log \mathbf{q}$, we utilize the optimization toolkit Cooper [15] from <https://github.com/cooper-org/cooper>. \mathbf{q} is initialized as a uniformed distribution, $\mathbf{q}(y) = \frac{1}{K}$ for all $y \in [K]$. We use the standard SGD as the primal and dual optimizers for 2000 steps.

B.6 Long-tail learning baselines and training details

We compared with 5 long-tailed classification methods:

1. Standard ERM: We learn the model by standard empirical risk minimization on the long-tailed data.
2. Learnable Weight Scaling (LWS) [24]: We first learn the model by standard ERM, then fix the model and learn to re-scale the magnitude of the classifier using class-balanced sampling.
3. Logit Adjustment (LA) [35]: We first learn the model by standard ERM, then compensates the long-tailed distribution by subtracting a class-dependent offset to the model outputs.
4. Balanced Softmax (BS) [43] modifies the Softmax cross-entropy loss which explicitly accommodate the label distribution shift during optimization.
5. BALLAD [33] first fine-tunes the vision-language models via contrastive loss on long-tailed data, then freezes the backbone and finally employs an adapter to enhance the representations of tail classes with re-sampling strategies.

For all combinations of the fine-tuning baselines and long-tailed learning methods, visual backbones are initialized from CLIP-ResNet-50 and all classifiers are initialized by feeding prompt with class names to the text encoder. We use SGD for all experiments with a momentum of 0.9 for 50 epochs with batch size of 512. The initial learning rate is set to 1.6×10^{-3} which is decayed by the cosine annealing rule. To mitigate explosive gradients, we use the warmup learning rate equals to 10^{-5} during the first epoch. For the sake of fairness in comparison, all hyper-parameters of baselines are carefully searched using grid search on the validation set.

C Additional Experiments

C.1 Few-shot learning accuracy

We provide mean and standard deviation in Table 9 in for {1, 2, 4, 8, 16} shots on all 11 few-shot learning datasets.

Dataset	1 shot	2 shots	4 shots	8 shots	16 shots
ImageNet	61.65 ± 0.15	62.64 ± 0.01	63.32 ± 0.07	64.51 ± 0.09	65.61 ± 0.03
Caltech101	89.08 ± 0.09	90.25 ± 0.25	90.98 ± 0.43	91.90 ± 0.21	92.58 ± 0.42
OxfordPets	87.79 ± 0.15	87.86 ± 0.21	88.22 ± 0.21	88.09 ± 0.27	89.53 ± 0.16
StanfordCars	60.00 ± 0.14	63.10 ± 0.42	66.25 ± 0.19	69.87 ± 0.09	73.95 ± 0.11
Flowers102	73.45 ± 0.60	81.00 ± 0.46	88.31 ± 0.65	92.89 ± 0.46	95.41 ± 0.32
Food101	78.41 ± 0.07	78.62 ± 0.07	78.68 ± 0.06	78.85 ± 0.19	79.54 ± 0.47
FGVCAircraft	20.22 ± 0.59	22.09 ± 0.37	24.65 ± 0.85	28.23 ± 0.44	31.99 ± 0.50
SUN397	64.29 ± 0.19	66.32 ± 0.16	68.01 ± 0.08	69.99 ± 0.18	71.64 ± 0.21
DTD	47.38 ± 1.23	50.75 ± 1.46	56.90 ± 0.20	62.73 ± 0.80	65.78 ± 0.49
EuroSAT	56.50 ± 1.34	67.26 ± 3.58	72.40 ± 2.43	77.59 ± 1.84	84.93 ± 1.89
UCF101	65.32 ± 0.17	68.42 ± 0.81	70.88 ± 0.50	74.23 ± 0.24	76.07 ± 0.03

Table 9: GLA Accuracy (%) with standard deviation of few-shot learning on 11 datasets.

C.2 Experiments on LAION-400M

To support our thought experiment in the discussion of Section 4.3, we use the Open-CLIP ViT-B/16 [21], the first 20k image in LAION-400M datasets and the bias estimation method proposed by [2] to estimate the expected logits across 8 classes: “dog”, “cat”, “squirrel”, “tiger”, “elephant”, “horse”, “pig” and “bird”. The bias estimation proposed by [2] provides a good estimation of $\log P(\mathbf{x})$ over the labels under pre-training distribution. Our GLA estimates the label bias matches the downstream domain, we consider two downstream domain styles, *i.e.*, “photo” and “sketch” from DomainNet [38] dataset. For each domain, we randomly sampled 50 images for each class.

Method	dog	cat	squirrel	tiger	elephant	horse	pig	bird
expected logits by [2]	0.059	0.039	0.043	0.053	0.043	0.062	0.061	0.028
π_p by “photo”	0.059	0.041	0.047	0.055	0.048	0.062	0.060	0.033
π_p by “sketch”	0.059	0.043	0.063	0.061	0.067	0.042	0.047	0.056

Table 10: Comparison among different bias estimation using Open-CLIP-ViT-B/16.

We present the expected logits estimated by [2], along with the one calculated from “photo” and “sketch” downstream domain data in Table 10. Since the softmax is invariant to constant offsets, *i.e.*,

Method	Sketch	Real Photo
Zero-shot Open-CLIP	92.25	97.00
Debiased by [2]	89.50	97.50
Debiased by GLA	93.00	97.75

Table 11: Performance on sketch and real photo domain.

$\text{softmax}(\mathbf{x} + c) = \text{softmax}(\mathbf{x})$, we align the three label bias to yield the same logits on “dog” class by subtracting constant values. We observe that the label bias estimated by the "photo" domain align closely with [2] due to its close resemblance to the pre-trained domain. Conversely, the "sketch" image style, which significantly differs from the pre-training domain, results in a more pronounced deviation in the pre-trained label bias.

Additionally, we apply the three estimated label biases to debias the zero-shot model and evaluate the classification performance. The results are shown in Table 11, where the superiority of our method becomes evident on “sketch” domain (93.00% vs 92.25%). Applying the label bias from [2] on the "sketch" domain degrades the model’s performance (from 92.25% to 89.50%). This is attributed to the overall pre-training label bias does not adequately reflect the bias specific to the “sketch” domain.